CONFINEMENT AND EXPANSION MODELS FOR NONLINEAR ANALYSIS OF REINFORCED CONCRETE MEMBERS

Dr. Khalid S. Mahmoud
Prof.
Baghdad University

Dr. Ihsan Al-Shaarbaf
Assistant Prof.
Al-Nahrain University

Dr. Abbas A. Allawi
Lecturer
Baghdad University

ABSTRACT

This research pertains to expand the formulation and applicability of using confinement and expansion due to Poisson's ratio models for three dimensional non-linear finite element analysis of reinforced concrete members. A plasticity based model that acknowledges the asymmetric response of reinforced concrete under multiaxial stress conditions is used to account for the strength improvement under conditions of triaxial compression. Complex behavior of concrete such as compression softening and tension softening are incorporated to simulate concrete behavior. **DIANA** software is used for finite element analysis with the inclusion of confinement and expansion effects. The concept of material pre-strains is extended to accommodate modeling of the Poison's ratio effect. The applicability of the suggested confinement and expansion models are verified by comparing the results of Kupfer and Vecchio – Collins tests on shear panels with that obtained from **DIANA** software. These comparisons illustrate the ability of the confinement and expansion models to obtain the response of reinforced concrete members subjected to multiaxial stress conditions.

KEYWORDS

Compressive behavior, Confined concrete model, DIANA software, Expansion model, Finite element.

الخلاصة

في هذا البحث تم صياغة و تطبيق نموذج للحصروالتوسع بسبب نسبة بواسون في التحليل اللا خطي الثلاثي الابعاد باستخدام طريقة العناصر المحددة. جرى استخدام النموذج اللدن تحت تاثير حالة اجهاد متعدد المحاورلبيان مدى تاثير التحسن في مقاومة الخرسانة لاجهادات الانضغاط . كذلك جرى الاخذ بنظر الاعتبار تاثير تطرية الانضغاط وتطرية الانفعال للشد وتاثير الخرسانة ذات المقاومة العالية. تم استعمال برنامج **DIANA** للتحليل مع اخذ تاثير الحصر والتوسع بنظر الاعتبار. ان فكرة الانفعال المسبق تم استخدامها لبيان تاثير التوسع الناتج من نسبة بواسون. لبيان مدى تطبيقية استخدام نموذجي الحصر والتوسع المقترحين فقد جرى مقارنة نتائج فحوصات كوبفروفيشكو – كولنز لبلاطات خرسانية مع تلك المستحصلة من التحليل باستخدام برنامج **DIANA** . المقارنة بينت قابلية نموذجي الحصروالتوسع المقترحين على عكس تصرف الاعضاء الخرسانية المسلحة المعرضة الى حالات اجهاد متعدد المحاور بصورة جيدة.

INTRODUCTION

In concrete constitutive modeling, a number of different approaches have been used to calculate the material stiffness matrix. Traditionally, constitutive models for concrete have concentrated on reproducing the experimental observed nonlinear response of reinforced concrete specimens. Many constitutive models for multiaxial stress states are based on modifications to the uniaxial stress –

strain response. Concrete strength and stiffness are sensitive to multiaxial stress conditions. Ultimate strength and ductility are known to be significantly improved in the presence of lateral compressive stress which inhibits the propagation of microcracks (Figure (1)). Some modifications are required to extend the cracked concrete theory from two to three dimensions while a model is needed for material subjected to triaxial compressive stresses. To describe the response of reinforced concrete, models are required for strength degradation due to cracking, strength enhancement because of confinement and expansion due to effect of Poisson's ratio, pre and post-peak stress-strain response in tension and compression.

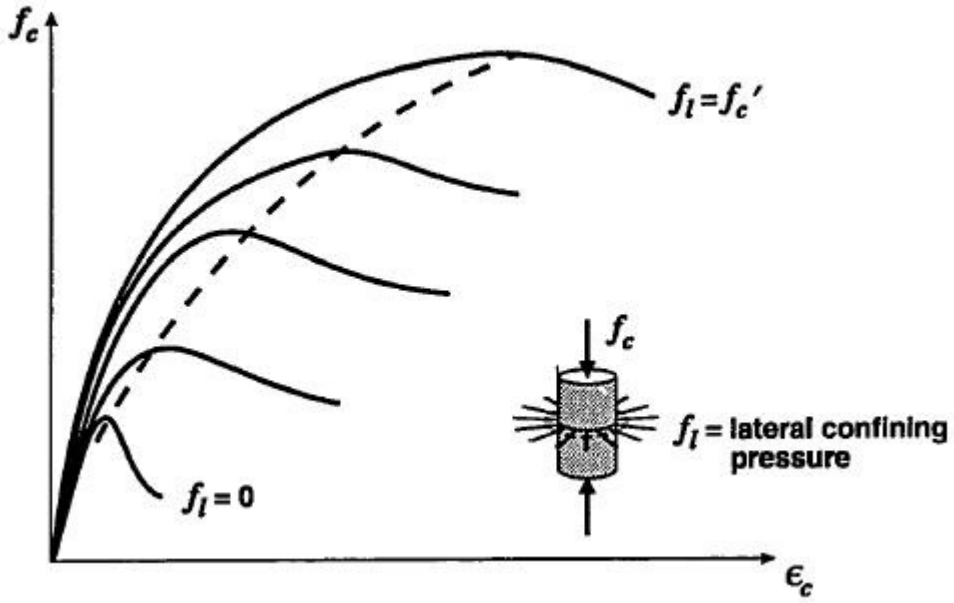

Fig (1): Effect of confinement on strength and ductility of concrete [Chen 1982].

STRESS - STRAIN CURVES FOR COMPRESSIVE RESPONSE

The constitutive equations for multiaxial stress state are based on modifications to the concrete uniaxial stress – strain curve. The Hognestad parabola describes the stress – strain response of a normal strength cylinder loaded in uniaxial compression. The parabolic relationship to determine the compressive stress f_{c3} corresponding to the compressive principal strain ε_{c3} (Vecchio and Collins 1982) is:

$$f_{c3} = \begin{cases} -f_p \left[2\left(\dfrac{\varepsilon_{c3}}{\varepsilon_p}\right) - \left(\dfrac{\varepsilon_{c3}}{\varepsilon_p}\right)^2 \right] & , 0 > \varepsilon_{c3} > \varepsilon_p \\ -f_p \left[1 - \left(\dfrac{\varepsilon_{c3} - \varepsilon_p}{2\varepsilon_0 - \varepsilon_p}\right)^2 \right] & , \varepsilon_p > \varepsilon_{c3} > 2\varepsilon_o \end{cases} \quad (1)$$

where f_p and ε_p are the peak stress and the strain at peak stress, respectively. The strain at peak stress is calculated as $2 f_c'/E_c$ where E_c is the initial slope to the parabola. For the case of uniaxial compression, the peak stress will be the cylinder strength f_c' which occurs at the strain ε_o

The uniaxial stress – strain response of high strength concrete is more linear in the ascending branch and the descending branch drops more sharply as shown in Figure (2). Therefore, the Hoghnestad parabola does not provide a good representation of the response of high strength

concrete. Also, in low strength concrete ($f_c' <$ 20 MPa), the Hognestad parabola tends to underestimate stresses at intermediate levels (Vecchio and Collins 1993). Thus, various alternatives were considered. It was found that the Thorenfeldt et al. (1987) model resulted in a good correlation for the full range of concrete strength represented in the database. The Thorenfeldt base curve later was calibrated by Collins and Porasz (1989) and as follows:

$$f_{c3} = f_p \cdot \frac{\varepsilon_{c3}}{\varepsilon_p} \cdot \frac{n}{n-1+(\varepsilon_{c3}/\varepsilon_p)^{nk}} \quad (2)$$

where n is given by:

$$n = 0.8 + \frac{f_c'}{17} \quad (3)$$

and k equals 1 for ascending branch, and

$$k = 0.67 + \frac{f_c'}{62} \quad (4)$$

for the descending branch (where f_c' is in MPa). For this curve, the strain at peak stress under uniaxial compression is estimated as:

$$\varepsilon_0 = \frac{n}{n-1} \cdot \frac{f_c'}{E_c} \quad (5)$$

The effect of the cylinder strength on the shape of this curve is shown in Figure (2).

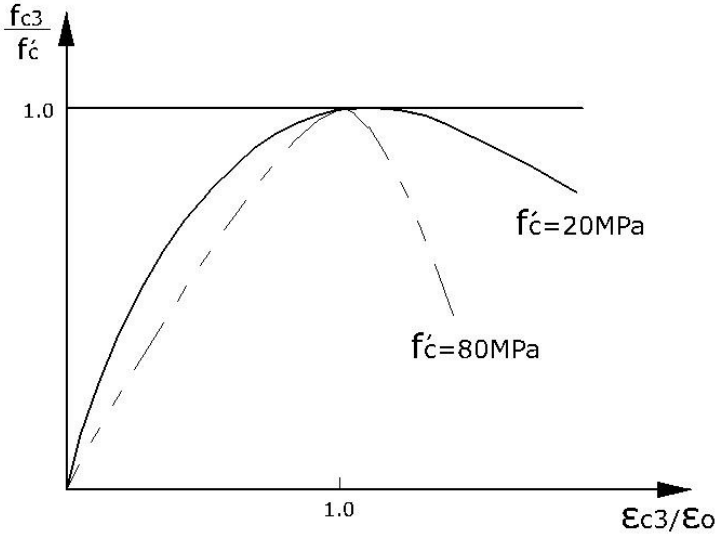

Fig (2): Effect of f_c' on the shape of curve given by Eq. (2) (Collins and Porasz 1989).

CONFINED CONCRETE MODEL

Lateral confining stresses increase the strength, stiffness and strain at peak stress of concrete cylinders. The strength enhancement is modeled by modifying the peak stress of the base curve. The failure surface proposed by Hsieh et al. (1979) is:

$$2.0108 \frac{\sqrt{J_2}}{f_c'^2} + 0.9714 \frac{\sqrt{J_2}}{f_c'} + 9.1412 \frac{f_{c1}}{f_c'} + 0.2312 \frac{I_1}{f_c'} - 1 = 0 \quad (6)$$

is used to find the stresses required in the major compressive direction to cause failure, f_{c3f} , in the presence of the stresses f_{c1} and f_{c2}. The invariants J_2 and I_1 are defined in terms of the stress f_{ci} in concrete according to:

$$J_2 = \frac{1}{6}\left((f_{c1}-f_{c2})^2 + (f_{c2}-f_{c3})^2 + (f_{c3}-f_{c1})^2\right) \quad (7)$$

$$I_1 = f_{c1} + f_{c2} + f_{c3} \quad (8)$$

and f_{c1} is the tensile principal stress in concrete.
The multipliers in this equation are curve fitting factors chosen to represent the results of a number of tests (Chen 1982). The stress f_{c3f} is used as the peak stress of the base curve and a peak stress factor , K_σ is defined as:

$$K_\sigma = \frac{f_{c3f}}{f_c'} \tag{9}$$

while experimental evidence suggests the same factor can be applied to find the peak stress and the corresponding peak strain in cracked concrete, different factors must be applied to f_c' and ε_o for confined concrete. The peak strain increases much more rapidly than the peak stress as confining pressure is increased. To relate the peak stress factor and the strain at peak stress factor, K_ε, a two part expression is implemented as shown in Figure (3). For low peak stress ratios ($K_\sigma < 3$), a fit to the data of Kupfer et al. (1969) is used.

$$K_\varepsilon = 0.2036\ K_\sigma^{\,4} - 2.819\ K_\sigma^{\,3} + 13.313 K_\sigma^{\,2} - 24.42\ K_\sigma + 13.718\sqrt{K_\sigma} + 1 \tag{10}$$

And for peak stress ratios, the expression is:

$$K_\varepsilon = 5\ K_\sigma - 4 \tag{11}$$

The coordinates of the apex of the base curve become

$$f_p = K_\sigma \cdot f_c' \tag{12}$$

$$\varepsilon_p = -\varepsilon_0 \left[K_\sigma \left(1 - \frac{f_{c3}}{f_{c3f}} \right) + K_\varepsilon \left(\frac{f_{c3}}{f_{c3f}} \right) \right] \tag{13}$$

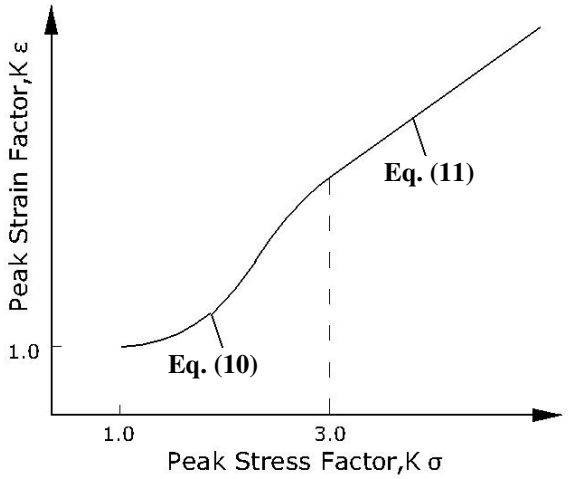

Fig (3): Peak stress and corresponding peak strain in confined concrete.

The ratio f_{c3} / f_{c3f} is a measure of the degree of nonlinearity. When this value is low, the strain at peak stress is close to $K_\sigma\ \varepsilon_o$. At ultimate strength level, the strain at peak stress becomes closer to $K_\varepsilon\ \varepsilon_o$. The modified stress – strain curve is then used to determine all three concrete stresses from the corresponding principal strains. Increased ductility is evident when concrete is confined. To simulate the descending branch given in Figure (4) of the stress – strain curve of confined concrete, a liberal modification was made to modify Kent – Park model (Scott et. al. 1982). The descending branch is given by:

$$f_{c3} = -f_p \left[\ 1 + Z_m \left(\varepsilon_{c3} - \varepsilon_p \right) \right] \quad \leq \quad -0.2 f_p \tag{14}$$

where

$$Z_m = \frac{0.5}{\frac{3+0.29 f_c'}{145\ f_c' - 1000} \cdot \left(\frac{\varepsilon_0}{-0.002}\right) + \left(\frac{-I_1 + f_{ci}}{170}\right)^{0.9} + \varepsilon_p} \tag{15}$$

I_1 is the first stress invariants, f_{ci} is the current stress in the principal direction under consideration, and ε_o and ε_p are negative quantities. This equation is in S.I. units.

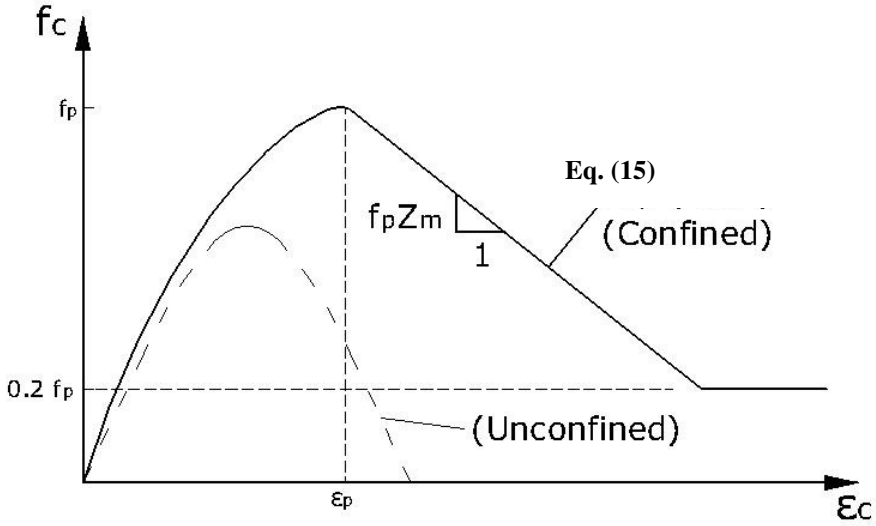

Fig (4): Compressive stress-strain model for confined concrete.

Lateral expansion increases rapidly near the peak stress as shown in Figure (5). At compressive stresses close to failure, the Poisson's ratio can exceed 0.5 (i.e., volume increasing). This behavior is modeled by a fit to the Kupfer et al. (1969) as follows:

$$\nu_{ij} = \begin{cases} \nu_0 & ;\ 0 > \varepsilon_{cj} > \dfrac{\varepsilon_p}{2} \\ \nu_0 \left[1 + 1.5\left(\dfrac{2\varepsilon_{cj}}{\varepsilon_p} - 1\right)^2\right] \le 0.5 ; & \dfrac{\varepsilon_p}{2} > \varepsilon_{cj} \end{cases} \tag{16}$$

where υ_o ratio is the initial Poisson's ratio. This relationship implies that only three Poisson's ratios are independent since:

$$\left.\begin{aligned} \nu_{21} &= \nu_{31} \\ \nu_{12} &= \nu_{32} \\ \nu_{13} &= \nu_{23} \end{aligned}\right\} \tag{17}$$

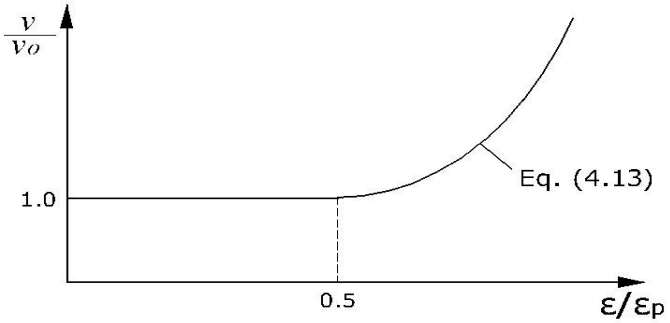

Eq. (16)

Fig (5): Increase in Poisson's ratio close to peak stress.

For uncracked concrete in tension, the initial Poisson's ratio is used. Upon cracking in the tensile principal direction, expansion normal to this direction is set to zero only. (i.e., $\upsilon_{21} = \upsilon_{31} = 0$, but all other Poisson's ratio are nonzero). If the intermediate principal direction also cracks, υ_{12} and υ_{32} are set equal to zero. All Poisson's ratios are zero if three orthogonal tensile failures occur (i.e., cracked concrete case).

In the current work, concrete cracking is based on the smeared model approach with plasticity model. It is simulated by an elastic-plastic work hardening response (based on Thorenfeldt base curve) followed by a perfectly plastic plateau which is terminated at the onset of crushing.

EXPANSION EFFECT

The Poisson effect of a material determines the lateral displacement of a specimen subjected to a uniaxial tensile or compressive loading. If these displacements are constrained, a passive lateral confinement will act on the specimen. This effect is considered important in a three-dimensional modeling of reinforced concrete structures. This effect is modeled through a pre-strain concept in which the lateral expansion effects are accounted for with an additional external loading on the structure with 2-dimensional nature (Vecchio 1992). Cracked concrete treated using the smeared crack approach is inherently modeled as an orthotropic material. In confined concrete, the adoption of an orthotropic model allows for the consideration of anisotropic behavior close ultimate. The three dimensional orthotropic material stiffness matrix can be written in the principal directions (Weaver and Johnston 1984) as:

$$[D_c]' = \frac{1}{\phi}\begin{bmatrix} E_1(1-\nu_{32}\nu_{23}) & E_1(\nu_{12}+\nu_{13}\nu_{32}) & E_1(\nu_{13}+\nu_{12}\nu_{23}) & 0 & 0 & 0 \\ E_2(\nu_{21}+\nu_{31}\nu_{23}) & E_2(1-\nu_{31}\nu_{13}) & E_2(\nu_{23}+\nu_{21}\nu_{13}) & 0 & 0 & 0 \\ E_3(\nu_{31}+\nu_{21}\nu_{32}) & E_3(\nu_{32}+\nu_{12}\nu_{31}) & E_3(\nu_{23}+\nu_{21}\nu_{13}) & 0 & 0 & 0 \\ 0 & 0 & 0 & \phi G_{12} & 0 & 0 \\ 0 & 0 & 0 & 0 & \phi G_{23} & 0 \\ 0 & 0 & 0 & 0 & 0 & \phi G_{31} \end{bmatrix} \quad (18)$$

where E_i is the modulus of elasticity in the *i*-direction and the Poisson's ratio ν_{ij} is the component of strain in the *i*-direction due to a stress in the *j*-direction and

$$\phi = 1-\nu_{32}\nu_{23}-\nu_{21}\nu_{12}-\nu_{31}\nu_{13}-\nu_{21}\nu_{32}\nu_{13}-\nu_{31}\nu_{12}\nu_{23} \quad (19)$$

The three shear moduli are given by:

$$G_{12} = \frac{E_1 E_2}{E_1(1+\nu_{12})+E_2(1+\nu_{21})} \quad (20)$$

$$G_{23} = \frac{E_2 E_3}{E_2(1+\nu_{23})+E_3(1+\nu_{32})} \quad (21)$$

$$G_{13} = \frac{E_1 E_3}{E_1(1+\nu_{13})+E_3(1+\nu_{31})} \quad (22)$$

To maintain symmetry in the stiffness matrix, the following three conditions must be satisfied:

$$E_1\nu_{12} = E_2\nu_{21} \quad (23)$$

$$E_2\nu_{23} = E_3\nu_{32} \quad (24)$$

$$E_1\nu_{13} = E_3\nu_{31} \quad (25)$$

In cracked concrete, most orthotropic material descriptions (i.e., smeared crack models) have assumed that the Poisson's ratio effect is negligible. All of diagonal terms in Eq. (18) become zero since the six Poisson's ratios are neglected, i.e., $\nu_{ij} = 0$. This assumption is relatively good for many cases, but for the case in which the tensile strains in cracked concrete are relatively small, the lateral

expansion of concrete arising from Poisson's ratio effect can be predicted in this situation. Also, in triaxial compressive stress conditions the Poisson's ratio effect cannot be neglected.

This concept is also applied to the nonlinear material model implemented in **DIANA** software. Provisions were included to model pre-strains arising from strain offset effects such as pre-stressing of reinforcement, shrinkage or expansion of concrete and thermal expansion of either concrete or reinforcement. For concrete, a pre-strain vector is $\{\varepsilon_c{}^o\}$ defined relative to the global x, y, and z system as:

$$\{\varepsilon_c{}^o\}=\{\varepsilon_{cx}{}^o \;\; \varepsilon_{cy}{}^o \;\; \varepsilon_{cz}{}^o \;\; \gamma_{cx}{}^o \;\; \gamma_{cy}{}^o \;\; \gamma_{cz}{}^o\}^T \tag{26}$$

accounting for all nonstress related straining. A similar vector developed for the reinforcement pre-strains. An equivalent force approach was then used to incorporate the pre-strain effects. From the known pre-strains, free nodal displacements $\{r_c\}$ and $\{r_s\}$ were calculated for the concrete and steel, respectively:

$$\{r_c\}=\int\{\varepsilon_c{}^o\}\,dV \tag{27}$$

$$\{r_s\}=\int\{\varepsilon_c{}^o\}\,dV \tag{28}$$

The equivalent nodal loads due to the pre-strains, $\{F^*\}$ can be calculated as:

$$\{F^*\}=[k_c]\{r_c\}+\sum_{i=1}^{n}[k_s]_i\,\{r_s\}_i \tag{29}$$

where $[k_c]$ and $[k_s]_i$ are the element stiffness matrices evaluated separately for the concrete and each reinforcement component. These equivalent nodal forces due to the pre-strains are then added to the externally applied nodal forces to determine the total nodal forces. The total nodal load vector is updated on each iteration since the equivalent nodal forces depend on the component stiffness. This algorithm will be modified here to include the expansion effect due to Poisson's ratio effect. The expansion strains in the principal directions are written as:

$$\{\varepsilon_{c\rho}{}^o\}=\{\varepsilon_{c1}{}^o \;\; \varepsilon_{c2}{}^o \;\; \varepsilon_{c3}{}^o\}^T \tag{30}$$

where

$$\varepsilon_{c1}{}^o=-\nu_{12}\frac{f_{c2}}{E_{c2}}-\frac{\nu_{13}\,f_{c3}}{E_{c3}} \tag{31}$$

$$\varepsilon_{c2}{}^o=-\nu_{21}\frac{f_{c1}}{E_{c1}}-\frac{\nu_{23}\,f_{c3}}{E_{c3}} \tag{32}$$

$$\varepsilon_{c3}{}^o=-\nu_{31}\frac{f_{c1}}{E_{c1}}-\frac{\nu_{32}\,f_{c2}}{E_{c2}} \tag{33}$$

The expansion strains are then transformed to the global x, y, and z axes according to:

$$\{\varepsilon_c{}^o\}=[T]\{\varepsilon_{c\rho}{}^o\} \tag{34}$$

where [T] is the transformation matrix that defines the orientation of the principal axes. Equivalent nodal loads are calculated as outlined in Eq. (29) to include all straining arising from expansion in the right hand side of Eq. (35).

$$[K]\{r\}=\{F\} \tag{35}$$

All of the expansion strains are modeled through the pre-strain concept so the material stiffness matrix then includes diagonal terms only.

$$[D_c]' = \begin{bmatrix} E_{c1} & 0 & 0 & 0 & 0 & 0 \\ 0 & E_{c2} & 0 & 0 & 0 & 0 \\ 0 & 0 & E_{c3} & 0 & 0 & 0 \\ 0 & 0 & 0 & G_{c12} & 0 & 0 \\ 0 & 0 & 0 & 0 & G_{c23} & 0 \\ 0 & 0 & 0 & 0 & 0 & G_{c13} \end{bmatrix} \quad (36)$$

where E_{c1}, E_{c2} and E_{c3} are the tangent modulus.

$$E_{c1} = \frac{f_{c1}}{\varepsilon_1} \quad (37)$$

$$E_{c2} = \frac{f_{c2}}{\varepsilon_2} \quad (38)$$

$$E_{c3} = \frac{f_{c3}}{\varepsilon_3} \quad (39)$$

and the shear modulus are given by:

$$G_{c12} = \frac{E_{c1}\ E_{c2}}{E_{c1} + E_{c2}} \quad (40)$$

$$G_{c23} = \frac{E_{c2}\ E_{c3}}{E_{c2} + E_{c3}} \quad (41)$$

$$G_{c13} = \frac{E_{c1}\ E_{c3}}{E_{c1} + E_{c3}} \quad (42)$$

The principal strains used in Eqs. (37 – 39) are that part of strains occurred due to direct stress. That is, any nonstress-related strains are first subtracted from the total strains before calculating the principal values. The pre-strains approach is valid for both uncracked and cracked concrete. An iterative procedure is required for finite element analysis based on this approach.

CRACKED CONCRETE MODEL

Cracked reinforced concrete is treated as an orthotropic nonlinear material based on a smeared rotating crack model. In cracked concrete, large strains perpendicular to the principal compressive direction reduce the concrete compressive strength. Thus, the compressive stress f_{c3} is a function of εc1 in addition to ε_{c3}. The compression softening factor, λ, is given by:

$$\lambda = \frac{1}{0.85 - 0.27\left(\frac{\varepsilon_{c1}}{\varepsilon_{c3}}\right)} \leq 1.0 \quad (43)$$

where ε_{c1} is the tensile principal strain.

The above compression softening relationship was derived by (Vecchio and Collins 1982) from tests on reinforced concrete panels of normal strength concrete. Also, high strength concrete is thought to exhibit a more pronounced compression softening effect due to smoother fracture planes. The compression softening factor was updated (Vecchio and Collins 1993) based on statistical evaluations of data, the strength and strain softening model shown in Figure (6) is referred as Model A and takes the form:

$$\lambda = \frac{1}{1 + K_s \cdot K_f} \leq 1.0 \quad (44)$$

where

$$K_s = 0.35\left(\frac{-\varepsilon_{c1}}{\varepsilon_{c3}} - 0.28\right)^{0.8} \geq 1.0 \quad (45)$$

$$K_f = 0.1825\sqrt{f_c'} \quad (46)$$

and f_c' is expressed in MPa. The K_s factor accounts for the effect of the transverse straining and K_f represents the influence of the concrete cylinder strength. The peak stress and strain of the base curve are modified to account for the effect.

$$f_p = \lambda . \ f_c' \quad (47)$$

$$\varepsilon_p = \lambda . \varepsilon_o \quad (48)$$

After that, only slightly weaker correlation was obtained by using a strength only softening model as a function of $\varepsilon_{c1.}$ The optimal form attained, referred to as model B (Vecchio and Collins 1993) which is adopted in this research and illustrated in Figures (7) and (8), is:

$$\lambda = \frac{1}{1 + K_c} \leq 1.0 \quad (49)$$

where

$$K_c = 0.27\left(\frac{\varepsilon_{c1}}{\varepsilon_0} - 0.37\right) \quad (50)$$

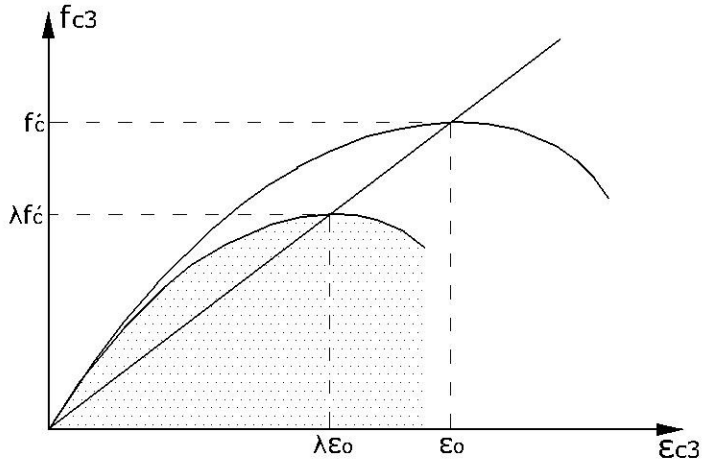

Fig (6): Model A for compression softening (Vecchio and Collins 1993).

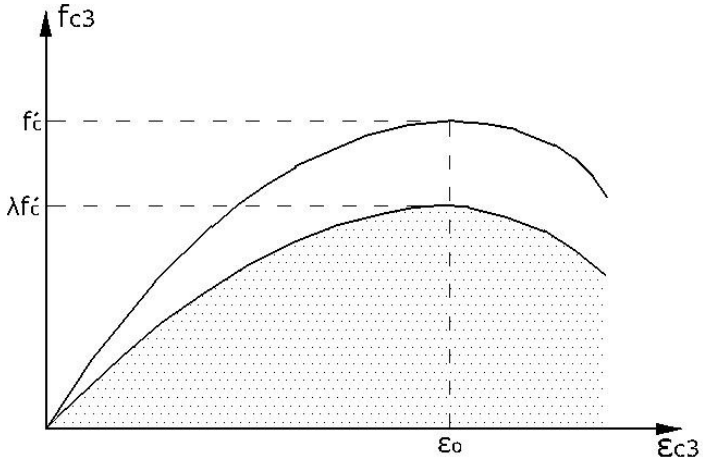

Fig (7): Model B for compression softening (Vecchio and Collins 1993).

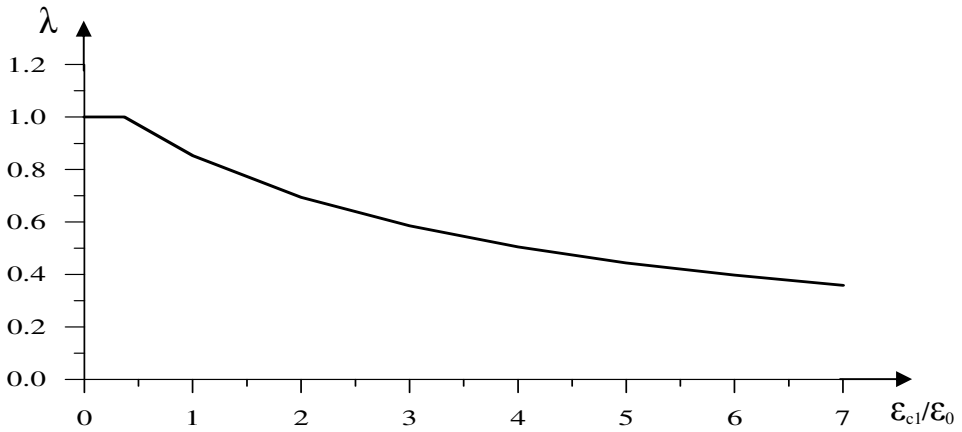

Fig (8): Model B for compression softening due to lateral cracking , Eq. (49) (Vecchio and Collins 1993).

In tension, a strain softening model is used by adopting the behavior which is based on a bilinear stress-strain relationship (Hillerborg et al. 1976) and as shown in Figure (9).

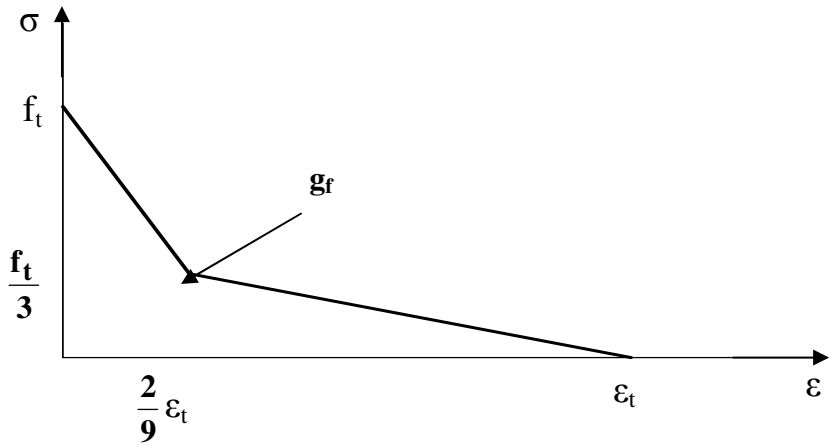

Fig (9): Hillerborg et al strain softening model (Hillerborg et al. 1976)

The shear stiffness at a cracked sampling point becomes progressively smaller as the crack widens. So the shear modulus is reduced to β *G.* Before cracking, the factor β is set equal to 1.0. When the crack is sufficiently opened, a constant value is assigned to β, to account for the dowel action as shown in Figure (10). The following relations are used to account for the shear retention effect (Al-Shaarbaf 1990).

$$\beta = 1.0 \quad \text{for } \varepsilon_n \le \varepsilon_{cr}$$

$$\beta = \frac{(\gamma_2 - \gamma_3)}{(\gamma_1 - 1.0)} \cdot \left(\gamma_1 - \frac{\varepsilon_n}{\varepsilon_{cr}} \right) + \gamma_3 \quad \text{for } \varepsilon_{cr} \le \varepsilon_n \le \gamma_1 \varepsilon_{cr} \tag{51}$$

$$\beta = \gamma_3 \quad \text{for } \varepsilon_n > \gamma_1 \varepsilon_{cr}$$

where $\gamma 1$, γ_2 and γ_3 are the shear retention parameters. γ_1 represents the rate of decay of shear stiffness as the crack widens, γ_2 represents the sudden loss in the shear stiffness at the onest of cracking, and γ_3 represents the residual shear stiffness due to the dowel action.

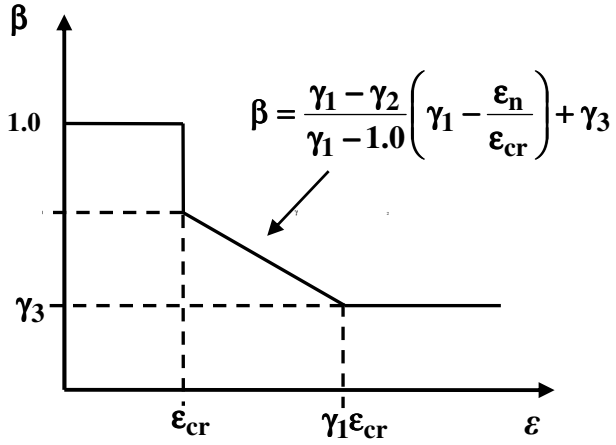

Fig (10): Shear retention model for concrete (Al-Shaarbaf 1990).

MODELING OF REINFORCEMENT

Modeling of reinforcing steel in connection with the finite element analysis of reinforced concrete members is much simpler than the modeling of concrete. The steel bars are long and relatively slender, and therefore, they can be assumed to transmit axial force only. In the current work, the embedded reinforcement model with an elastic-linear work hardening model is adopted to simulate the uniaxial stress-strain behavior of reinforcing steel bars, Figure (11).

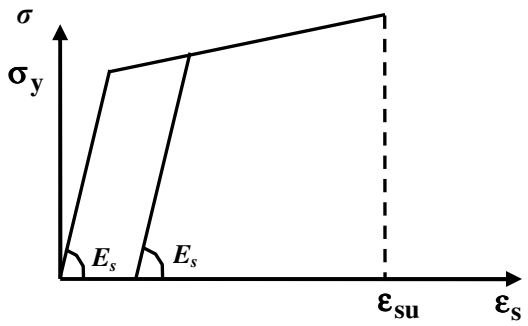

Fig (11): Stress-strain relationship of reinforcing steel bars (Al-Shaarbaf 1990).

FORMULATION OF FINITE ELEMENT ANALYSIS

In the present study, the computer software, **DIANA V9.0** (Witte and Kikstra, 2002), has been adopted to carry out the numerical analysis. The main objective of the study is to analyze some experimental cases to verify the use of both the confining and expansion models and as follows:

A - CONCRETE IDEALIZATION

The 20-node hexahedral brick element is used in the current study to model the concrete. Each node of this element has three translation degrees of freedom u, v and w in the x, y and z directions respectively as shown in Figure (12) (Al-Shaarbaf 1990). The element employs the standard shape functions to define the displacement field (Dawe 1984). The displacements of the brick element are given by:

$$u(\xi,\eta,\zeta)=\sum_{i=1}^{20} Ni(\xi,\eta,\zeta).u_i$$
$$v(\xi,\eta,\zeta)=\sum_{i=1}^{20} Ni(\xi,\eta,\zeta).v_i \qquad (52)$$
$$w(\xi,\eta,\zeta)=\sum_{i=1}^{20} Ni(\xi,\eta,\zeta).w_i$$

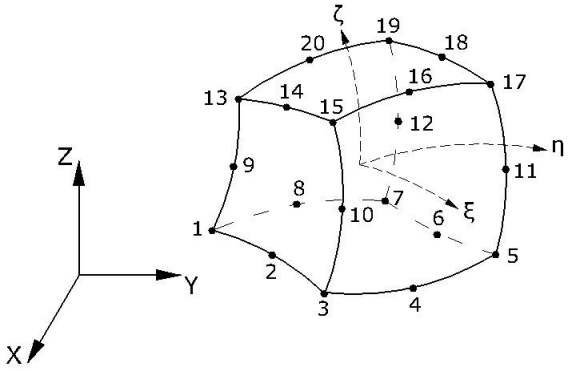

Fig (12): 20-Nodded isoparametric brick element

B - REINFORCING BAR IDEALIZATION

The reinforcing bars are idealized as axial members embedded within the brick elements (Zeinkiwecz 1977). Reinforcing bars are assumed to be capable of transmitting axial force only. The stiffness matrix of steel bars is added to that of the concrete to obtain the global stiffness matrix of the brick element. The shape functions of the brick element can be used to represent the displacements of the embedded bar (Al-Shaarbaf 1990). For example,

$$u=\sum_{i=1}^{20} Ni(\xi).u_i$$
$$v=\sum_{i=1}^{20} Ni(\xi).v_i \qquad (53)$$
$$w=\sum_{i=1}^{20} Ni(\xi).w_i$$

where a bar is considered lying parallel to the local coordinate axis ξ with $\eta=\eta_c$ and $\zeta=\zeta_c$ (constant), Figure (13).

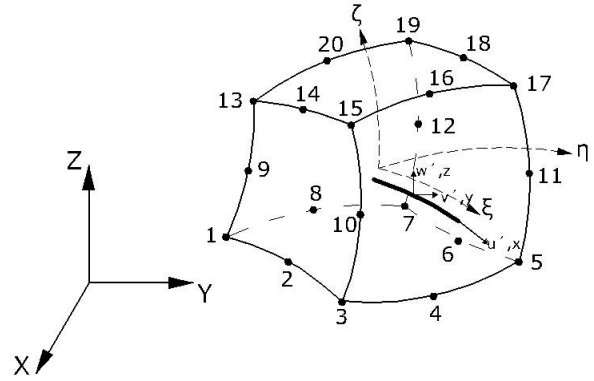

Fig (13): Representation of embedded reinforcement.

C- General Nonlinear Solution Procedure

The incremental-iterative method is the most common technique used for solving nonlinear structural equations. Loading on the studied specimens is induced by means of a prescribed displacement at the point load. The numerical integration has been conducted by using the 27 points Gaussian rule (3x3x3).

VERIFICATION WITH EXPERIMENTAL RESULTS

A – Confined Concrete Model

The data collected by Kupfer, Hilsdorf and Rusch (Kupfer et. al 1969) from a series of plain concrete specimens tested under different combinations of in plane biaxial loading were selected to establish the ability of proposed model for confined concrete under multiaxial compressive stresses. The 200 mm square and 50 mm thick specimens subjected to biaxial compression were selected. The plain concrete had cylinder strength of 18.7 MPa. Further concrete properties are shown in Table (1). Analysis was carried out using **DIANA** for lateral confining stress equal to zero (i.e., uniaxial compression), $\sigma_3 / 2$ and σ_3 (i.e., equal biaxial compression). The ratio of lateral to axial stress, σ_2 / σ_3 was held constant throughout the test. The out of plane stress σ_1 was zero in all three tests. Also another analysis was made but without including the effect of confinement. For biaxial compression, the volumetric strain (i.e., $\Delta V/V = .\varepsilon_1 + \varepsilon_2 + \varepsilon_3$) for various stress ratios (f_{c3}/f_c) are shown in Figure (14). The response, including the peak stress and strain at peak stress, was well duplicated in all cases. Also, the expansion was realistically reflected even near ultimate. It was noted that confined concrete model was capable of adequately obtaining the strength and deformation response under multiaxial stresses of the plain concrete.

B – Expansion Model

Two of Vecchio – Collins shear panels (Vecchio 1982) were selected to show the improvement in modeling that can realize when the Poisson's ratio effect is included in the cracked concrete theory. The normal strength panels, PV23 and PV25, were 890mm square by 70mm thick and symmetrically reinforced with two layers of wire mesh of 50mm grid. A clear cover of 6 mm was provided. They were equally reinforced in the longitudinal and transverse directions ($\rho_x = \rho_y =$ 1.875%, see Table (1)) and were loaded in shear and equal biaxial compression. No reinforcement yielded in either specimen before failure by crushing of the concrete. The improvement is evident in Figures (15) and (16) which shows the results of analyses using **DIANA** with and without the expansion model. It was noted that the effect of expansion on the load deformation response is to increase the strength and to increase the stiffness near ultimate. Little influence is apparent at low and intermediate stress levels.

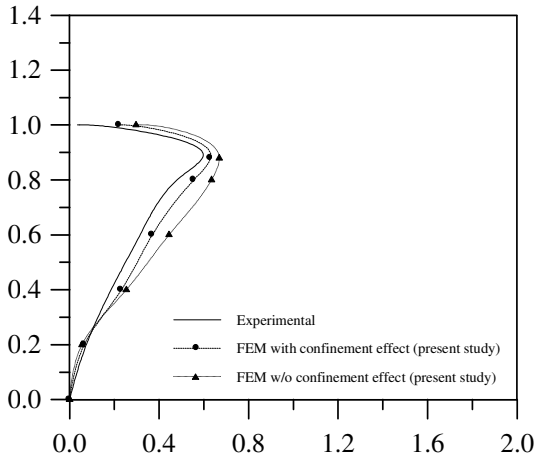

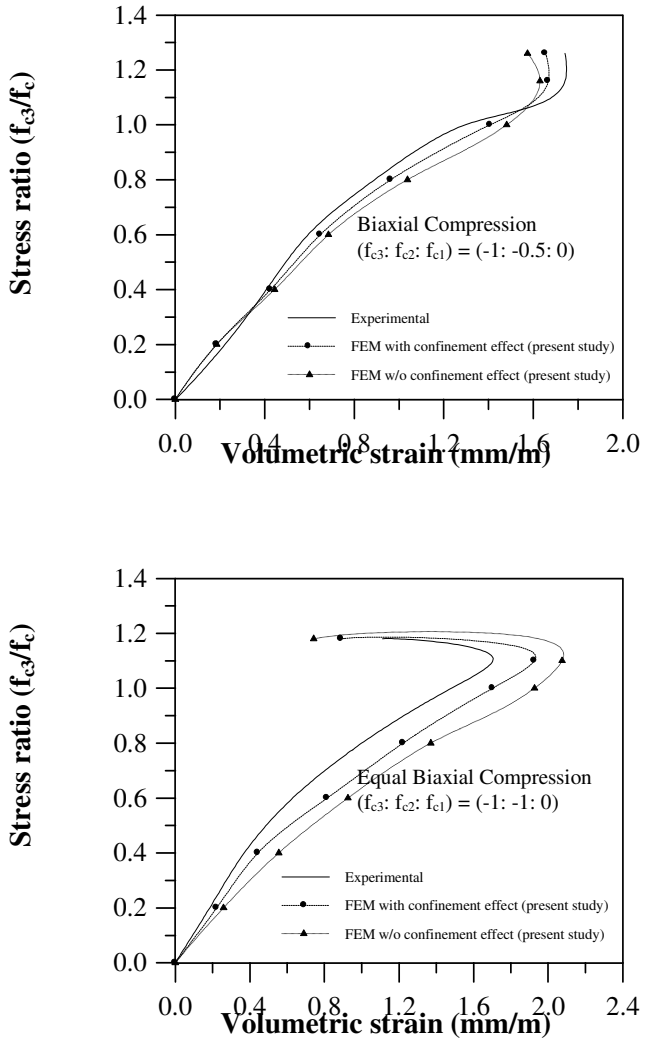

Fig (14): Volumetric response of the Kupfer et al. analysis

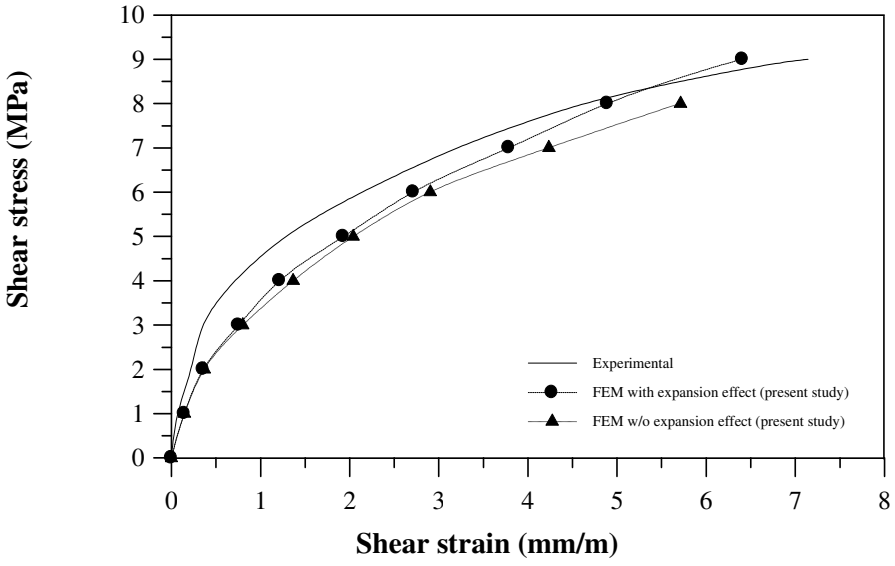

Fig (15): Influence of expansion Effect for Panel (PV23) (Vecchio 1982).

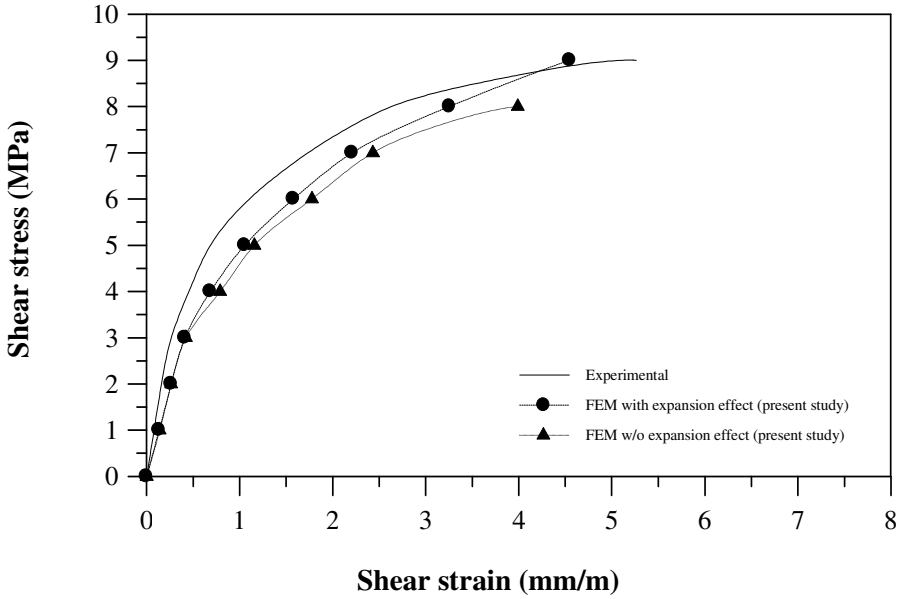

Fig (16): Influence of expansion Effect for Panel (PV25) (Vecchio 1982).

Table (1): Specimens properties

Specimen	f_c' ,MPa	f_t,MPa	ε_o	ν_o	ρ_x , %	f_{yx},MPa	ρ_y , %	f_{yy},MPa
Kupfer et al.	18.7	1.46	0.002	0.15	-	-	-	-
PV23	20.5	1.5	0.002	0.3	1.785	518	1.785	518
PV25	19.2	1.45	0.002	0.3	1.785	466	1.785	466

CONCLUSIONS

Based on the analytical work, the following conclusions are made:

1- The proposed confined concrete model proved capable of providing good estimates of strength and deformations for concrete elements subjected to multiaxial compressive stresses. Applications of the model to finite element analyses were successful when behavior was sought on a "macroscopic" level.

2- The consideration of the Poisson's ratio effect can have a significant effect and has improved the accuracy near ultimate strength.

3- The consideration of the Poisson's ratio effect can have a significant effect when the tensile principal strain is relatively small.

4- The pre-strain approach handled the asymmetry of the material stiffness matrix in a numerical stable manner when including the effect of Expansion due to Poisson's ratio.

5- Both confinement and expansion effect can model the response of concrete members subjected to different load conditions.

REFERENCES

Al-Shaarbaf, I..(1990). "*A Non-Linear Three-Dimensional Finite Element Analysis.*" Ph.D. Thesis, University of Bradford.

Chen, W.F. (1982). "*Plasticity in Reinforced Concrete.*" McGraw-Hill, New York, USA.

Collins, M.P. , and Porsaz, A. (1989). "*Shear Strength for High Strength Concrete* ", Bull. No. 193 "*Design Aspects of High Strength Concrete.*" Committee Euro-International du Beton (CEB), pp. 75-83.

Dawe, D.J. (1984)."*Matrix and Finite Element Displacement Analysis of Structures.*" Clarendon Press, Oxford.

Hillerborg, A., Mondeer, M., and Petersson, P.E. (1976)." *Analysis of Crack Formation and Growth in Concrete by Means of Fracture Mechanics and Finite Elements.*" Cement and Concrete Research, V. 6, No. 6, 1976, pp. 773-782.

Hsieh, S.S., Ting, E.C., and Chen, W.F. (1979)." An Elastic *Fracture Model of Concrete.*" Proc. 3rd Engineering Division Spec. Conference , ASCE, Austin , Texas, pp. 137-440.

Kupfer, H. , Hilsdorf, K.H,. and Rusch, H.(1969). "*Behavior of Concrete Under Biaxial Stresses.*" Journal of the American Concrete Institute, V. 66, No. 8, pp. 656-666.

Scott, B.D., Park, R. and Priestley, M.J.N. (1982). "*Stress-Strain Behavior of Concrete Confined by Overlapping Hoops at Low and High Strain Rates.*" Journal of the American Concrete Institute, V. 79, No. 1, pp. 13-27.

Thorenfeldt, E. , Tomaszewicz, A. , and Jensen, J.J. (1987)." *Mechanical Properties of High Strength Concrete and Application in Design.*" Proc. Symposium Utilization of High Strength Concrete. Stavanger, Norway, Tapir Trondheim.

Vecchio, F.J., and Collins, M.P. (1982). " *The Response of Reinforced Concrete to in-Plane Shear and Normal Stresses.*" Publication No. 82-03, Dept. of Civil Engineering, University of Toronto, Canada.

Vecchio, F. J. (1992). "*Finite Element Modeling of Concrete Expansion and Confinement*." Journal of Structural Division, ASCE, Vol. 118, No.9-10, pp. 2390-2406.

Vecchio, F.J., and Collins, M.P. (1993). " *Compressive Response of Cracked Concrete.*" Journal of Structural Engineering , ASCE , V. 119, No.12 , 1993, pp. 3590-3610.

Weaver, W., J., and Johnston, P. R. (1984). "*Finite Elements for Structural Analysis.*" Prentic-Hall, Englwood Cliffs, N. J.

Witte, F.C. D., and Kikstra, W.P. (2002). "**DIANA** *Finite Element Analysis – User's Manual, Release 9.0.*" TNO Building and Construction Research, The Netherlands.

Zeinkiweicz, O.C. (1977). "*The Finite Element Method.*" Third Edition, McGraw-Hill, London, 1977.

NOTATIONS

$[D_c]'$	Concrete material stiffness matrix in principal direction
E_c	Modulus of elasticity of concrete (initial tangent modulus)
E_{c1}	Concrete tangent modulus in tensile principal strain direction
E_{c2}	Concrete tangent modulus in intermediate principal strain direction
E_{c3}	Concrete tangent modulus in compressive principal strain direction
E_s	Modulus of elasticity of reinforcing bars
f_c	Compressive principal stress in concrete
f_c'	Compressive strength of concrete cylinder
f_{c1}	Tensile principal stress in concrete
f_{c2}	Intermediate principal stress in concrete
f_{c3}	Compressive principal stress in concrete
f_{c3f}	Required f_{c3} to cause failure in presence of on f_{c1} and f_{c2}
f_p	Peak stress
f_t	Modulus of rupture
$\{F\}$	Structure nodal force matrix
$\{F^*\}$	Equivalent nodal loads due to prestrain
G	Shear modulus
G_{12}	Tangent shear modulus of concrete relative to 1,2 axes
G_{23}	Tangent shear modulus of concrete relative to 2,3 axes
G_{13}	Tangent shear modulus of concrete relative to 1,3 axes
g_f	Area under tensile stress-crack strain curve
I_2	Second invariant of stress vector
J_2	Second invariant of deviatoric stress tensor
K_c	Coefficient reflecting influence of transverse tensile straining (Model B)
K_f	Coefficient reflecting influence of nominal strength of concrete
K_s	Coefficient reflecting influence of transverse tensile straining (Model A)
K_σ	Peak stress factor
K_ε	Strain at peak stress factor
$[K]$	Structure stiffness matrix
$[k_c]$	Element stiffness matrix evaluated for concrete component
$[ks]_i$	Element stiffness matrix evaluated for i-direction reinforcement
n	Curve fitting factor
$\{r\}$	Structure nodal displacement matrix
$\{r_c\}$	Free nodal displacement due to concrete prestrain
$\{r_s\}$	Free nodal displacement due to steel prestrain
u,v,w	Displacement coordinates in x,y and z Cartesian coordinates
x,y,z	Cartesian coordinates
$[T]$	Transformation matrix
Z_m	Slope factor for post-peak compressive curve
β	Shear retension factor
$\gamma_1, \gamma_2, \gamma_3$	Shear retension parameters
$\Delta V/V$	Volumetric strain = $.\varepsilon_1 + \varepsilon_2 + \varepsilon_3$
ε_c	Compressive principal strain in concrete
ε_{cr}	Cracking strain
ε_{c1}	Largest principal tensile strain in concrete
ε_{c2}	Intermediate principal strain in concrete
ε_{c3}	Compressive principal strain in concrete
$\varepsilon_{c1}^{\ o}$	Concrete expansion strain in 1-direction

$\varepsilon_{c2}^{\ o}$	Concrete expansion strain in 2-direction
$\varepsilon_{c3}^{\ o}$	Concrete expansion strain in 3-direction
$\{\varepsilon_c^{\ o}\}$	Concrete pre-strain relative to global axis
$\{\varepsilon_{cp}^{\ o}\}$	Expansion strain in principal direction
ε_o	Strain in concrete cylinder at peak stress f_c' (a negative value)
ε_p	Strain at peak stress (a negative value)
ε_s	Strain in steel reinforcement
ε_{su}	Ultimate strain for steel reinforcement
$\{\varepsilon_s^{\ o}\}$	Smeared reinforcement pre-strain relative to global axis
ε_t	Tensile fracture strain
ε_1	Tensile principal strain
ε_2	Intermediate principal strain
ε_3	Compressive principal strain
λ	Concrete compression softening factor
ν	Poisson's ratio of linear isotropic material
σy	Yield stress of reinforcing bars
ν_{ij}	Component of strain in i-direction due to a stress in the j-direction
ν_o	Initial Poisson's ratio
γ_{xy}	Shear strain relative to x,y axes
γ_{yz}	Shear strain relative to y,z axes
γ_{zx}	Shear strain relative to z,x axes